JOURNAL OF MATERIALS SCIENCE 28 (1993) 329–336

Characterization of heterogeneous matrix composites using scanning acoustic microscopy

E. M. WOO, J. C. SEFERIS*
Polymeric Composites Laboratory, Department of Chemical Engineering, University of Washington, Seattle, WA 98195, USA

Acoustic microscopy was used to examine the morphology of multi-phase matrices and composites. The acoustic microscopy imaging could easily resolve the rubber domains dispersed within a thermosetting or thermoplastic continuous phase. However, because the thermoplastic and thermosetting phase domains had comparable elastic moduli, the resolution between them was not always clear. Rayleigh wave distortion of imaging remained as one of the serious limitations that needed to be overcome in order for this technique to be widely utilized in heterogeneous/anisotropic media. In its present form, the acoustic imaging technique can be used to augment other existing analytical tools in order to generate more detailed morphological information that is useful in understanding structure–property relationships for multi-phase toughened matrices used in advanced composites.

1. Introduction

Heterogeneous polymer blends and multi-phase thermosetting matrix resins for advanced composites are rapidly being developed as new materials with improved and versatile performance for demanding applications. So far, progress in improving the fracture toughness of high-temperature thermosetting resins has been quite limited. However, as novel toughening methodologies are being developed, there is impressive success documented in the literature for toughening thermosetting resins such as epoxies, dicyanates, and bismaleimides [1–4]. Control of phase separation during curing and morphological parameters such as phase domain sizes, size distribution, phase constituents, and interfacial adhesion between phase domains are critical in determining the bulk properties of multi-phase systems. It has been demonstrated that these parameters influence the deformation and fracture mechanisms, and therefore ultimately they influence the mechanical properties and fracture toughness of the composite systems that are primarily controlled by the heterogeneous-phase matrix properties [2].

The morphology of resin matrices is traditionally characterized with scanning electron microscopy (with or without back-scattered electron imaging or X-ray fluorescence mapping), optical microscopy, and transmission electron microscopy. In certain cases where the structure cannot be directly visualized, techniques such as neutron, small-angle X-ray, wide-angle X-ray, or light scattering are also used to determine the sizes and shapes of the phase domains. However, none of the microscopic techniques provide direct interrelations between the image and the mechanical properties exhibited by the multi-phase samples. A new imaging technique based on ultrasonic acoustic waves was recently developed, offering the potential for directly "seeing" both the elastic modulus and density of the microphases in the sample [5]. This is a particularly useful technique for studying the morphology of high-performance, multi-phase matrix resins, since most of these matrices contain micro-constituents of different moduli and/or density characteristics that can be conveniently revealed by the acoustic imaging technique. It was anticipated that this study would identify important areas in which the acoustic imaging technique could be used to augment existing analytical techniques to elucidate the composition and structure of toughened multi-phase polymeric materials. In addition, this study investigated several frontier applications using this emerging acoustic microscopy technique in morphological studies of heterogeneous matrices as well as the exhibited anisotropy of carbon fibre composites. Advantages of acoustic microscopy include high-contrast imaging that reflects details of material elastic properties. Additionally, the unique sub-surface imaging capability using acoustic microscopy can be very desirable for sub-surface morphology and flaw detection. Despite these advantages, anisotropic issues as viewed by the acoustic microscopy technique must still be resolved.

1.1. Background

Acoustic imaging has been recently developed and put into practice through several commercialized scanning acoustic microscopes. The principles of acoustic

* To whom correspondence should be addressed.

0022–2461

microscopy have been discussed in several published books and papers [5, 6]. Acoustic studies of materials include defect detection in metals and ceramics, biology and medicine, structure and bonding evaluation in electronic integral circuit chips and wafers, and crystal imperfection analysis in semi-conductor materials [7, 8]. In addition, Maclachlan *et al.* [9] have applied the acoustic microscopy technique to study rigid-rod molecular composites.

Two basic types of acoustic microscopy technique and hardware have developed in parallel: transmission and reflection. These are in some respects analogous to transmission and scanning electron microscopy, respectively. In transmission acoustic microscopy [10], also referred to as scanning laser acoustic microscopy (SLAM), high-frequency sound (up to about 100 MHz) is passed through thin samples, from a transmitting to a receiving transducer. In reflection acoustic microscopy, which was the only technique used in this investigation, even higher frequencies (0.8 GHz and above) were employed. Moreover, with this technique sound is transmitted and reflected by a single transducer. The reflection-type technique was used for this investigation primarily because of its higher resolution capability, even though penetration depth was sacrificed, a primary advantage of lower-frequency techniques such as SLAM and ultrasound.

The probe in reflection acoustic microscopy imaging is a high-frequency (GHz) elastic wave generated by a transducer at a relatively high pulse rate, 0.8–2.0 GHz. The generated wave is focused by an acoustic lens and transmitted to the sample surface via a liquid coupling medium (usually water) between the lens and the sample. The acoustic wave is then reflected back from the specimen surface, sometimes after partial penetration into the sample, and is collected by the same lens and transducer. The reflected signals must be sorted out by an electronic separator to distinguish between the surface-reflected wave from the transmitting wave and the reflection wave from the lens surface, by going through a matching network. After proper sorting, the reflection wave from the specimen is processed into an acoustic image, which can reveal detailed information based on the moduli and densities of micro-constituents in the samples. In terms of its sub-surface detection capability, acoustic microscopy operates in much the same manner as radar or sonar for detection of submerged objects, and in much the same manner as ultrasound scanners for imaging and medical diagnosis. However, the wavelengths used in radar or sonar are much too long, and therefore their resolution is too poor to have any applications in microscopy. Recent technologies have made it possible to design a transducer that can generate acoustic waves of high enough frequencies for practical applications in microscopy with a potential resolution of 1 μm or less.

Even though there are still limitations, the new acoustic technique has the potential for use in interesting new materials characterization applications. Currently, the maximum magnification of acoustic microscopy is only about 2000× times with water couplant. Also, the imaging technique is very sensitive to the destructive/constructive interferences caused by Rayleigh waves near the surface of the sample [11]. Additionally, because of attenuation limitations, there is a limit on the highest practical frequencies available with acoustic microscopy. As a result, there exists a limit on the attainable resolution power. The attenuation of the acoustic wave rapidly increases with increasing wave frequency and the lens focal length, as indicated by the expression

$$\frac{\text{Reflected wave intensity}}{\text{Transmitted wave intensity}} = 10^{-0.1av^2x} \quad (1)$$

where a is a constant ($= 1.6 \times 10^{-13}$ dB m^{-1} Hz^{-2} for water at 30 °C), n is the frequency and x is the focal length. In this study a frequency of 1.3 GHz was used most often since it provided a reasonable compromise between penetration depth, resolution power and wave attenuation. The object (the specimen) to be examined must be properly coupled to the acoustic lens through a coupling medium, usually water or alcohol, with a temperature from ambient up to 60 °C [12]. The upper temperature limit is determined by the boiling point of the coupling medium. The wave attenuation is lower at higher temperatures. However, operation at a higher temperature requires much greater care in procedures and sample preparations. For convenience, the experiments were mostly performed at ambient temperature since the wave attenuation at the frequency of 1.3 GHz did not demand a higher coupling temperature.

2. Experimental procedure

2.1. Materials

Several multi-phase neat resin systems that included bismaleimide, epoxy and dicyanate resins and their fibre-reinforced composites were investigated in this study. The dicyanate resin used was a bisphenol-E dicyanate resin (Hi-Tek Polymers, Inc.) modified with polysulphone (PSu) and/or CTBN rubber [1]. The epoxy resins used were several polysulphone and/or liquid rubber-modified epoxy mixtures of two different functionalities [13]. The bismaleimide (BMI) resin used was a silicone rubber-modified bismaleimide, Kerimid 70003 (Rhone Poulenc, Inc.) [2]. Additionally, two fibre-reinforced laminate samples were examined. One was a glass fibre-reinforced epoxy and the other was an AS-4 carbon fibre-reinforced polyetheretherketone (PEEK) laminate (APC-2) (Imperial Chemical Industries).

Specimen preparation required careful polishing. Specimens were polished down to a sub-micrometre 0.3 μm alumina grit size. The regular polishing procedures that were used in preparing specimens for optical microscopy were followed for the acoustic microscopy experiments [13].

2.2. Apparatus

The microscopy equipment used was an E. Leitz scanning acoustic microscope (ELSAM) [11]. This commercially available instrument is designed to scan the sample line by line, to produce a pseudo real-time,

two-dimensional image ($X-Y$ mode). Imaging can also be produced by using a combination of scanning and deflection modulation (DM), where the echo intensity is reproduced vertically on the screen for each image point, giving a pseudo three-dimensional image. This is called a DMV or simply DM mode. Both the $X-Y$ and DMV modes were used in this study for comparisons of imaging results.

Fig. 1 shows a schematic diagram of the transducer–lens combination, which is the "heart" of the acoustic microscopy instrument. The acoustic objective consists of a piezo-electric transducer and sapphire lens (Al_2O_3). The transducer is a microcrystalline zinc oxide (ZnO) layer, which can be excited between two gold electrodes to produce ultrasound waves. The top surface of the lens, to which the transducer is adjacent, is polished flat. In addition, the transducer–lens combination is shaped as a cone pointing down with a miniature concave spherical cavity ground on the very tip of the cone. The radius of the lens is usually 100 μm or smaller, approximately equal to the focal length of the lens (the focal length $x = 1.13\,r_o$, where r_o is the radius). The frequency range available on this instrument is between 0.1 and 2.0 GHz. To cover this wide frequency range, three different transducers have to be used. The frequency of the acoustic wave, along with the modulus and density of the sample, determine the resolution power of the acoustic imaging and the depth of penetration in the sample.

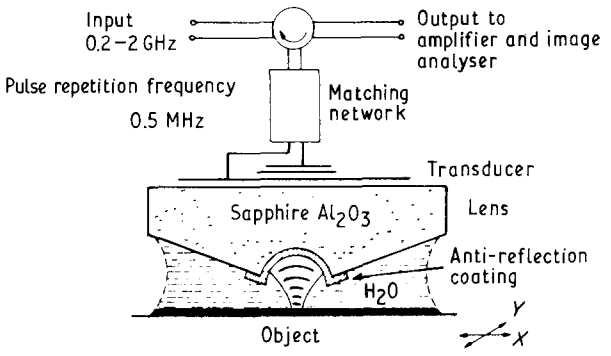

Figure 1 Schematic diagram of the transducer–lens combination of the acoustic microscope.

3. Results and discussion

Fig. 2 shows acoustic micrographs taken at 2000 × * ($X-Y$ mode) of the cross-section of a glass fibre-reinforced epoxy sample, oriented perpendicular to the fibre orientation that is a unidirectional laminate configuration. The acoustic images were generated with the lens focused on the surface, and re-focused 5 and 10 μm below the surface (shown in Fig. 2a, b and c, respectively). The bright circular spots correspond to the higher-elasticity glass fibre, while the dark "background" indicates the epoxy matrix domain that binds the fibres. For all the fibre images, there are concentric circular fringes with a 1.5–2.0 μm separation from each other. These fringes were caused by Rayleigh wave interference on the surface [9, 11]. The Rayleigh wave effect became more pronounced as the depth of focus increased. Also the contrast of imaging and the interfacial boundary between the fibre and the matrix became less clear as the sub-surface penetration increased.

Similarly, Fig. 3 shows the acoustic micrographs taken at 2000 × (DMV mode) of the carbon fibre-reinforced PEEK laminate (APC-2) sample, with the cross-section of the sample oriented at three different angles, 0, 30 and 45°, respectively, to the fibre orientation. Again, the bright domains are the fibre that has a much higher reflectivity to the acoustic wave, and the dark background represents the lower elastic modulus matrix PEEK domains. These images demonstrated that Rayleigh wave interference (a) was quite severe when the DMV mode was used in imaging and (b) increased with increasing angle of observation.

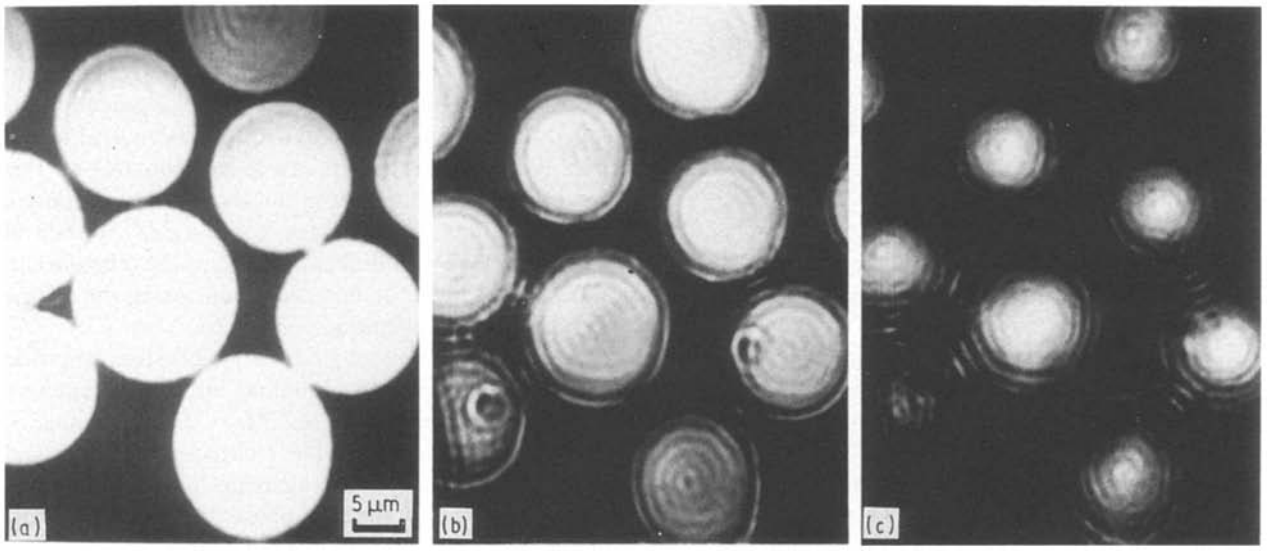

Figure 2 Acoustic micrographs (1.3 GHz, $X-Y$ mode) of glass–epoxy composite (a) at surface, (b) 5 μm and (c) 10 μm below the surface.

* Note that prints may have been reduced for reproduction.

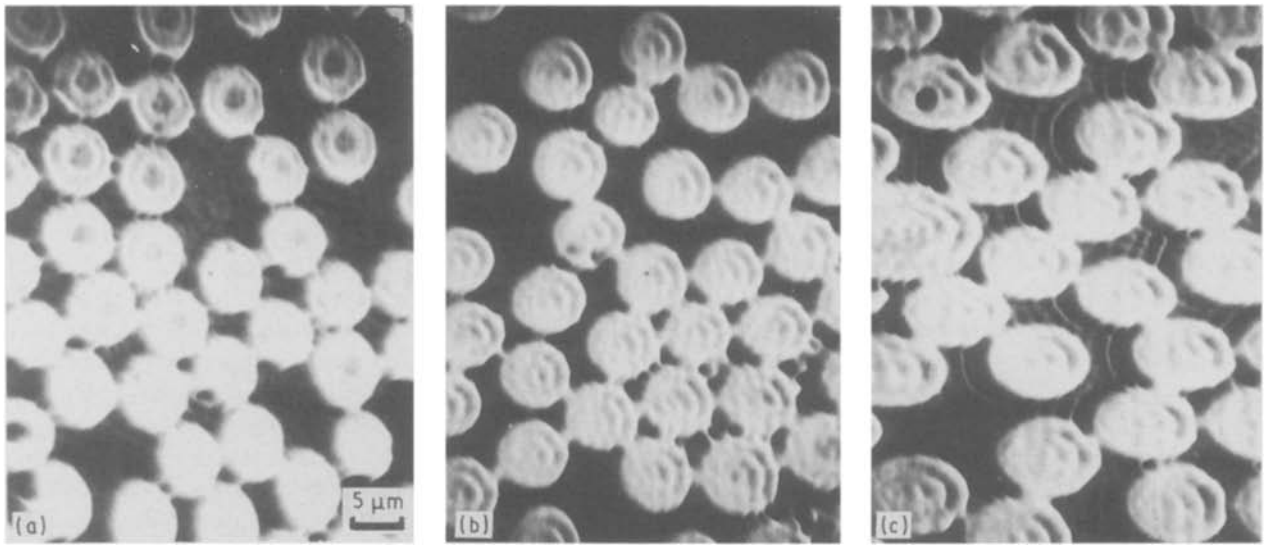

Figure 3 Acoustic micrographs (1.3 GHz, DMV mode) of carbon fibre–PEEK with fibre orientation at (a) 0°, (b) 30° and (c) 45°

Fig. 4 shows an acoustic micrograph of the polished surface of the sample of silicone-modified BMI taken at 2000 × using the X–Y mode and a 2 GHz frequency lens. An image produced before by the DMV mode exhibited severe distortion caused by Rayleigh wave interference, making identification of domains from the acoustic image virtually impossible. However, the acoustic image produced in the X–Y mode (Fig. 4) exhibited better results with a reasonable resolution. The BMI phase apparently formed continuous domains (the bright background). The circular, dark domains (2 to 10 μm in diameter) show some tiny particles (1 μm diameter or less) embedded in these domains, which could be attributed to a silicone-rich phase present in this system. These tiny particles embedded inside the spherical silicone rubber domains were probably from the BMI constituent. However, since the embedded particles were only 1 μm in size, the resolution power of acoustic microscopy was not good enough to allow unambiguous determination of the constituent nature of the particles embedded in the silicone domains. For example, these tiny images might also be attributed to voids created by volatile evolution during curing of silicone rubber-modified BMI [2]. These voids could be easily identified as the darker, but smaller (1–2 μm) domains with several concentric interference fringes in the image. By comparison, neither optical nor scanning electron microscopies were able to precisely distinguish the discrete silicone phase from the continuous BMI phase [2].

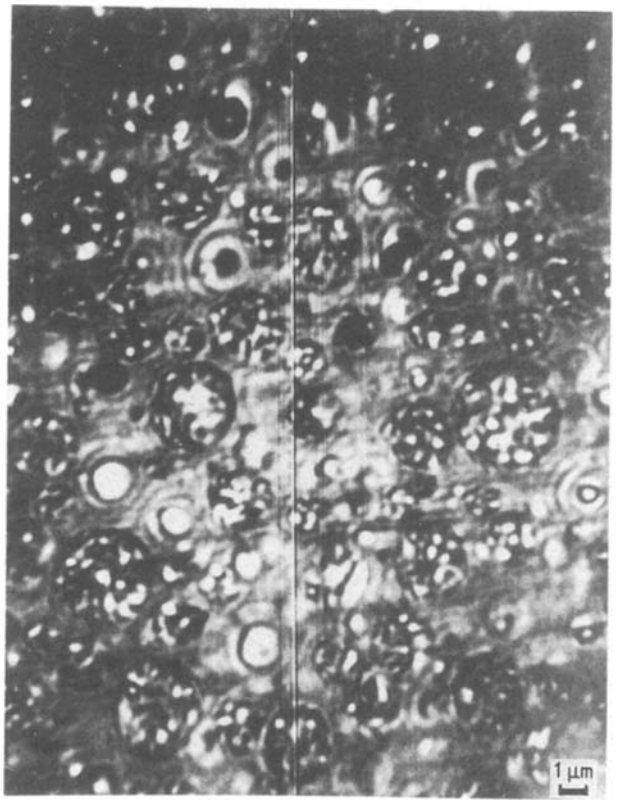

Figure 4 Acoustic micrograph (2 GHz, X–Y mode) of Kerimid 70003 BMI sample showing multi-phase/void structure.

Fig. 5 shows an acoustic micrograph (taken at 400 ×, 1.3 GHz, X–Y mode) of the dicyanate neat resin sample modified with 20 p.h.r. polysulphone. Other than some minor polishing defects, no heterogeneous phase morphology was detected by the acoustic microscopy technique. Even a maximum magnification of 2000 × (ELSAM equipment limit) failed to detect any heterogeneous phase morphology. The failure to resolve micro-phase domains in this sample might be due to the fact that the polysulphone and dicyanate phases have comparable moduli of elasticity, making it difficult to discern the difference in reflectivities from the micro-domains using the acoustic microscopy technique.

The same sample etched with methylene chloride was also examined using scanning electron microscopy (SEM) at a magnification of 2500 ×. The SEM micrograph is shown in Fig. 6. The etched surface as viewed using the SEM had a heterogeneous morphology. The SEM images show that the phase domains of dicyanate or thermoplastic polysulphone particles were 1 μm or smaller. Sub-micrometre domain sizes of the polysulphone or dicyanate particles are beyond the resolution power of the acoustic wave at 1.3 GHz. In this

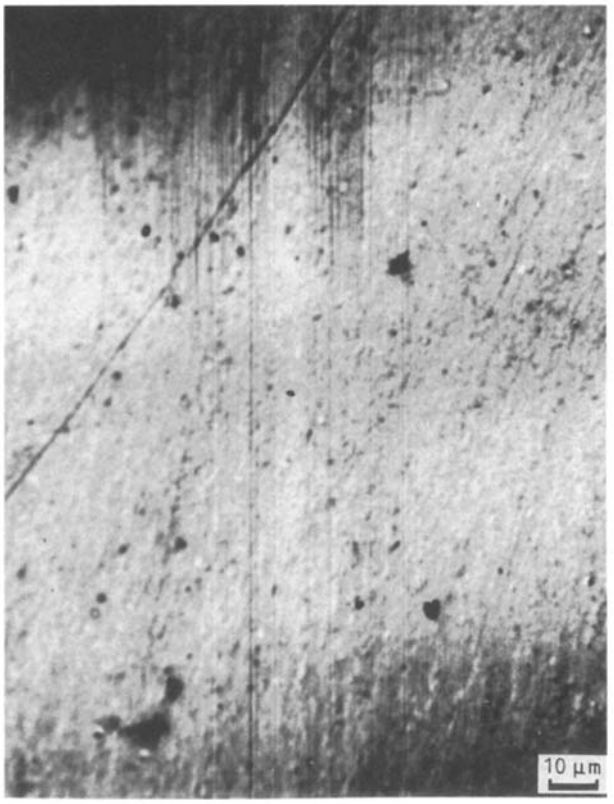

Figure 5 Acoustic micrograph (1.3 GHz, $X-Y$ mode) of polysulphone-modified dicyanate neat resin sample.

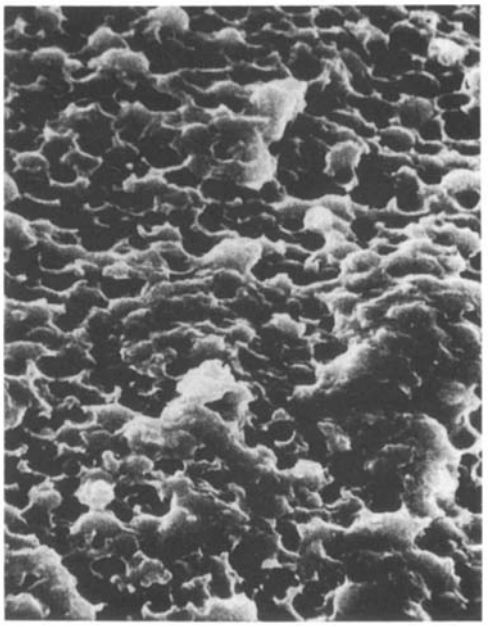

Figure 6 SEM micrograph of cured dicyanate–20% PSu etched with methylene chloride.

case, acoustic microscopy probably has no advantage over the scanning electron microscope.

Fig. 7a and b show the optical and acoustic images, respectively, of a dicyanate matrix sample modified with 25 parts PSu per hundred parts dicyanate (25 p.h.r.) and 5 p.h.r. of CTBN 1300 × 8 rubber. Comparing Fig. 7a and b, acoustic microscopy gave better contrast in the images than the optical microscopy. The rubber phase was seen as large (10–20 μm), dark, spherical domains of a uniform constituent. Particles-within-particles morphology was not observed for this sample, which contained 5 p.h.r. CTBN. However, as the CTBN rubber content was increased to 15 p.h.r. in the sample, the rubber domains in the dicyanate matrix grew much bigger (about 50–100 μm), and clearly

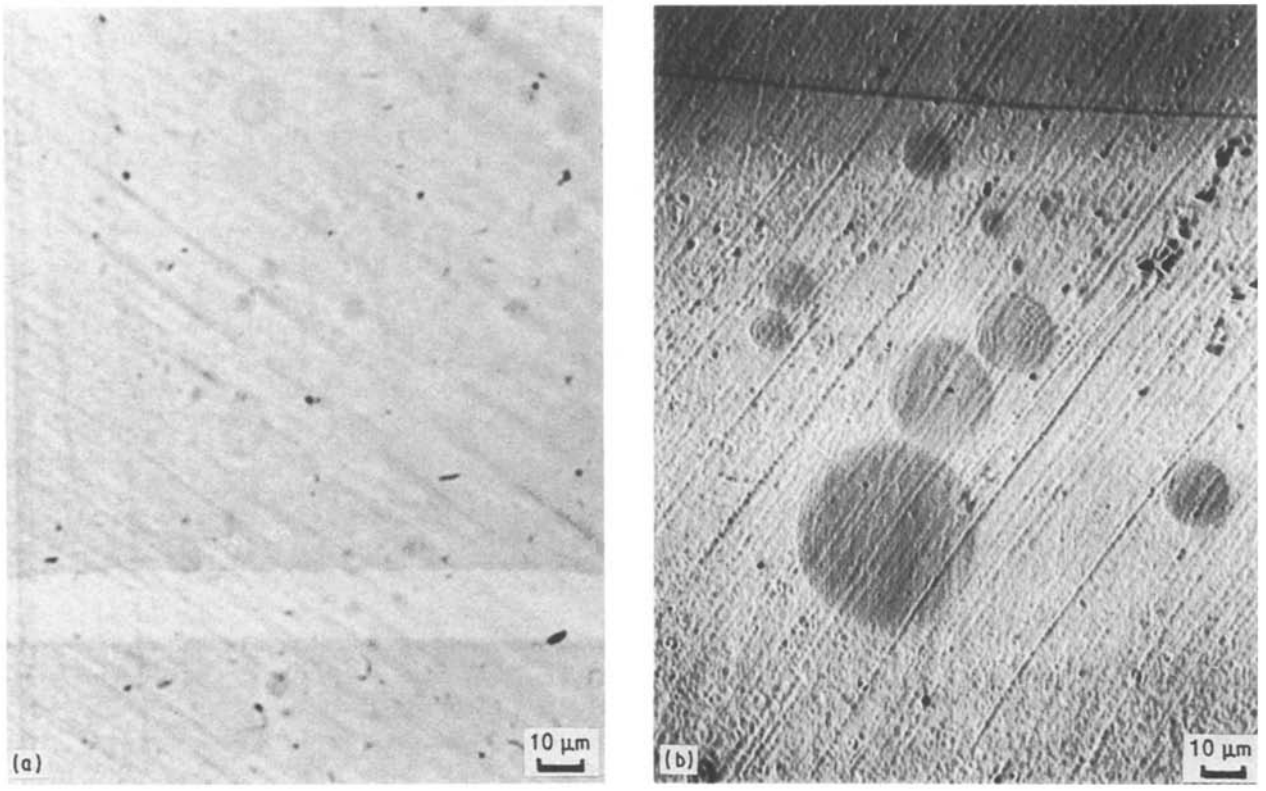

Figure 7 Dicyanate–PSu(25 p.h.r.)–CTBN × 8 (5 p.h.r.): (a) optical micrograph and (b) acoustic micrograph.

exhibited a phase-within-a-phase morphology of the rubber-rich domains, as shown in Fig. 8 (taken at $\times 625$). This is a characteristic feature for many rubber-modified or thermoplastic-modified thermosetting resins [13, 14]. The smaller particles trapped within the larger rubber particle were probably of dicyanate and/or PSu constituents. However, resolving the thermoplastic domains from the thermosetting domains was more difficult. For all the PSu–CTBN-modified dicyanate samples examined, the thermoplastic domains were not distinguishable using acoustic microscopy. As expected, for samples that incorporated the rubber component, the dramatic difference in the elastic moduli between the rubber and the dicyanate matrix greatly enhanced the contrast.

Fig. 9a and b show acoustic micrographs, taken at $400\times$ at the surface and $625\times$ at $-1\,\mu m$ below the surface, respectively, of the sample of rubber and thermoplastic-toughened epoxy matrix. Due to the relatively large sizes of the phase domains, identification of the phase domains by acoustic imaging was straightforward. Fig. 9a shows that the rubber-rich domains were resolved clearly as dark discrete domains of roughly spherical shape. The sizes of the discrete rubber domains ranged from 1 to 20 μm. Interestingly, thermoplastic-rich phase domains were also identified; these were represented by the semi-continuous grey area in the image. The thermoplastic constituent apparently formed the co-continuous phase along with the epoxy-rich constituent (the brighter area in the image). In summary, acoustic microscopy revealed that the thermoplastic and thermosetting components formed the co-continuous phase, while the rubber component formed the discrete phase domain with domain sizes ranging from 1 to 20 μm.

Fig. 9b shows the image of the same sample with the lens focused 1 μm below the sample surface. The contrast between the acoustic images of the thermoplastic and thermosetting phase domains decreased significantly, and only the rubber-rich area (the discrete dark domains) was still clearly visible. Generally, sub-surface penetration of the acoustic wave seemed to result in poorer contrast in imaging. This may be attributed to wave dispersion as a result of increased viscoelastic interference as the sound wave is focused under the sample.

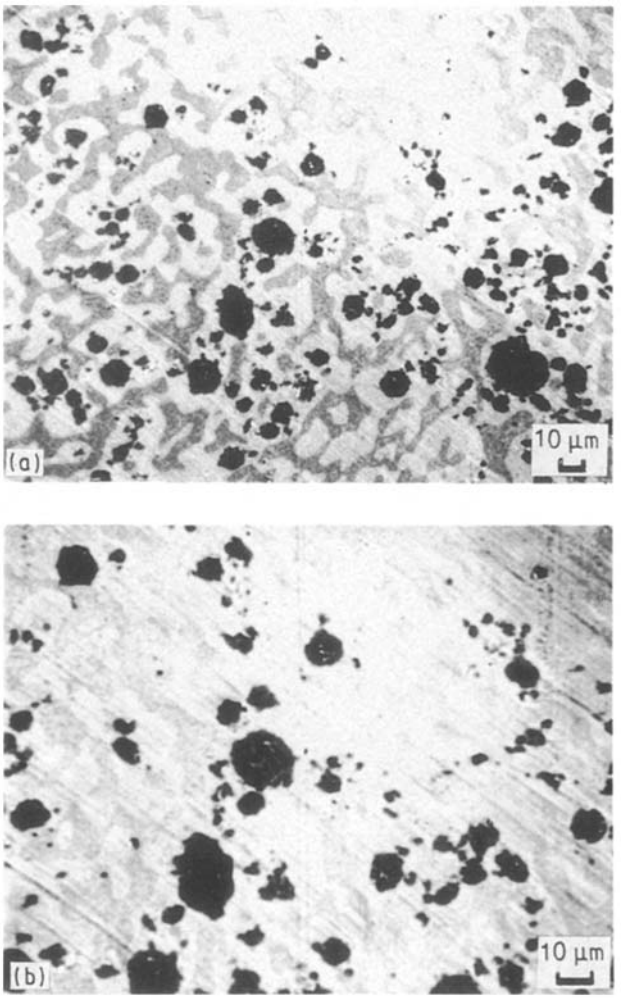

Figure 9 Acoustic micrographs (1.3 GHz, $X-Y$ mode) of rubber–thermoplastic-modified epoxy: (a) at surface, (b) 1 μm below the surface.

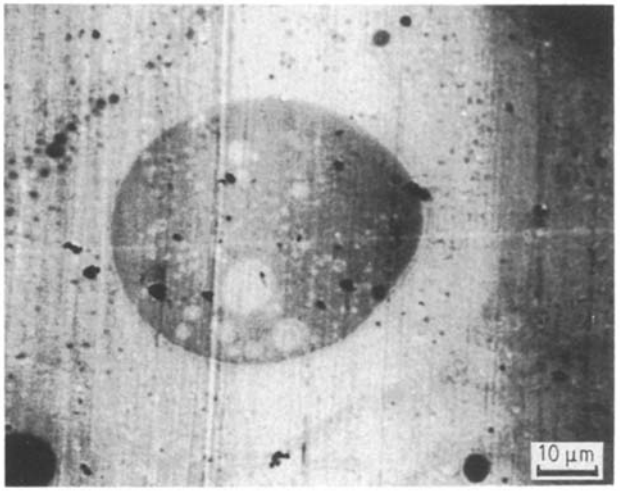

Figure 8 Acoustic imaging (1.3 GHz, $X-Y$ mode) of the sample of dicyanate modified with 20 p.h.r. of PSu and 15 p.h.r. CTBN.

Fig. 10 shows the acoustic micrograph of an epoxy sample toughened by 10 p.h.r. of PSu and 5 p.h.r. of ATBN, taken at $400\times$ magnification in the $X-Y$ mode. The rubber phase domains are apparently the dark spherical domains ranging from 1 to 10 μm in sizes. At 5 p.h.r. concentration of ATBN in the matrix, the rubber particles were uniformly dispersed in the continuous epoxy domains (the brighter background) with no agglomeration. Fig. 11 shows the acoustic micrograph (taken at $625\times$) of the same epoxy sample toughened by 10 p.h.r. PSu and 10 p.h.r. ATBN. At 10 p.h.r. concentration of ATBN in the matrix, the rubber particles were more heterogeneous in size. Apparently some smaller particles had agglomerated into larger ones. Furthermore, small particles aggregated and collapsed into a large one. When these small rubber particles eventually agglomerated into a large particle during curing, some epoxy constituent was likely to be trapped within the aggregating rubber particles during the agglomeration process. Con-

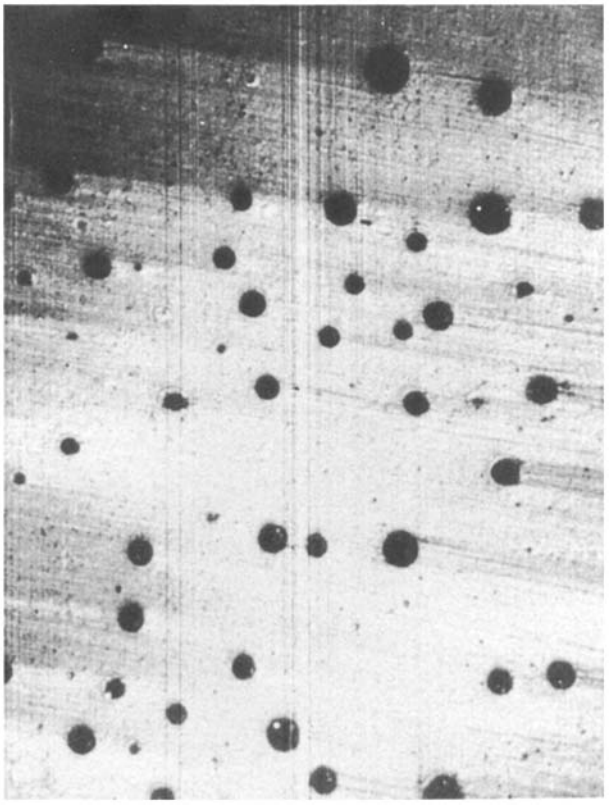

Figure 10 Acoustic micrograph (1.3 GHz, $X-Y$ mode) of sample of ATBN(5 p.h.r.)–PSu(10 p.h.r.)-modified HPT epoxy.

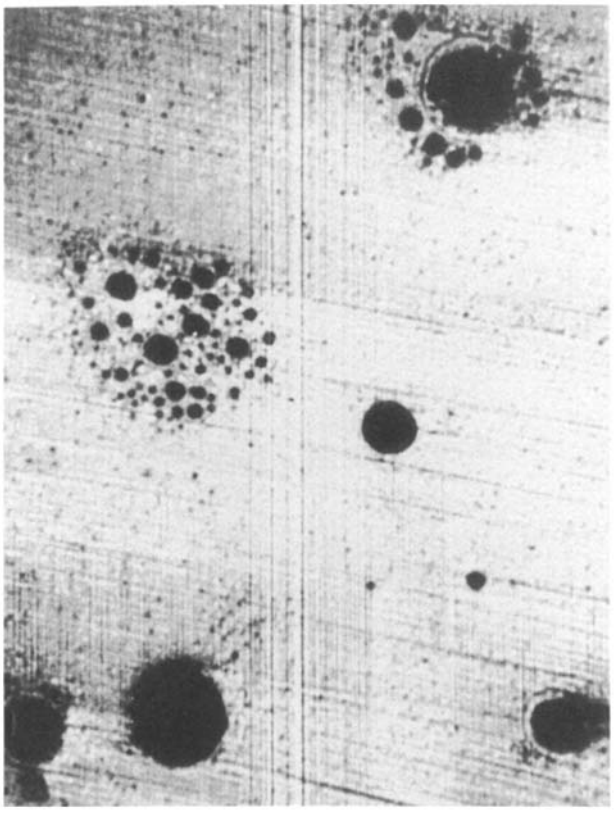

Figure 11 Acoustic micrograph (1.3 GHz, $X-Y$ mode) of sample of ATBN(10 p.h.r.)–PSu(10 p.h.r.)-modified HPT epoxy.

sequently, as shown, this is consistent with the phase-in-a-phase morphology, which has been generally observed in rubber-modified or thermoplastic-modified thermosetting matrices [13, 14].

4. Conclusion

The morphology of several high-temperature thermoplastic and thermosetting matrices and composites was characterized using the novel acoustic microscopy technique. Acoustic microscopy, which provides high-contrast images reflecting the modulus and density differences of the individual phase components, has definite advantages over conventional microscopic techniques for heterogeneous multi-phase matrix composites. Soft domains such as CTBN or silicone rubber, commonly used in multi-phase matrix resin systems, could be readily identified by acoustic microscopy due to the relatively large difference in the elastic moduli of the phase constituents of the multi-phase matrices. Currently, the capability of the acoustic microscope to develop high-contrast images can be exploited to identify micro-constituents in multi-phase systems, especially rubber-modified thermosetting resin matrices or engineering thermoplastics.

The sub-surface capability of acoustic microscopy may also be useful in detecting flaws, cracks, voids, or fibre–matrix interfacial bondings in matrix resins or composites. However, sub-surface capabilities were found to be hampered by rapidly decreasing resolution because of Rayleigh wave interference or wave attenuation. Furthermore, decreasing contrast was observed as the penetration increased. Detection of cracks, voids and crazes in fibre composites by using acoustic microscopy remains a potentially useful application if the Rayleigh wave interference can be properly accounted for in the imaging process.

Overall, when coupled with anisotropic elasticity theories for heterogeneous systems, acoustic microscopy has the potential of interrelating the morphological features to mechanical performance and durability. When the micro-phase components exhibited large differences in their elastic moduli, the identification of phase domains was found to be advantageous through acoustic imaging in its current form. Collectively, acoustic microscopy and imaging techniques can be expected to augment the existing analytical tools for more enhanced morphological characterization of heterogeneous anisotropic and viscoelastic systems, such as composites.

Acknowledgements

This study was part of an ongoing joint evaluation of acoustic microscopy by Boeing Materials Technology of the Boeing Company, E. Leitz of Germany, and the Polymeric Composites Laboratory of the University of Washington. The technical assistance in sample preparation provided by Mr Luther Gammon of Boeing and by Mr Garry Duschl for equipment operation and maintenance while on leave from Boeing to the Polymeric Composites Laboratory for this study, was greatly appreciated. Expert coordination provided by Dr G. Faulhaber of E. Leitz and Dr A. G. Miller of Boeing Commercial Airplane Group is gratefully acknowledged. Financial assistance provided through project and material support by the industrial sponsors of the Polymeric Composites Laboratory made the evaluation possible.

References

1. E. M. WOO, B. K. FUKAI and J. C. SEFERIS, Proc. Amer. Soc. Comp. 3rd Tech. Conf. (1988) 192.
2. J.-F. VIOT and J. C. SEFERIS, *J. Appl. Polym. Sci.* **34** (1987) 1459.
3. I. GAWIN, in Proceedings of 31st International SAMPE Symposium "Materials Science for the Future" (SAMPE International, Covina, 1986) p. 1204.
4. S. TAKEDA and H. KAKIUCHI, *J. Appl. Polym. Sci.* **35** (1988) 1351.
5. A. BRIGGS, in "An Introduction to Scanning Acoustic Microscopy", Royal Microscopical Society, Microscopy Handbook, Vol. 12 (Oxford University Press, New York, 1985).
6. B. HADIMIOGLU and C. F. QUATE, *Appl. Phys. Lett.* **43** (1983) 1006.
7. R. S. GILMORE, K. C. TAM and D. R. HOWARD, *Phil. Trans. R. Soc. London* **A320** (1986) 215.
8. C. ILETT, M. G. SOMEKH and G. A. D. BRIGGS, *ibid.* **A393** (1984) 171.
9. J. W. MACLACHLAN, M. MADEY, R. K. EBY and W. W. ADAMS, *Polym. Commun.* **28** (1987) 326.
10. L. W. KESSLER and D. E. YUHAS, *Scanning Electr. Microsc.* **1** (1978) 555.
11. A. THAER, M. HOPPE and W. J. PATZELT, "The ELSAM Acoustic Microscope", Sonderdruck aus Leitz Mitteilungen fur Wissenschaft u. Technik, Vol. 8, No. 3/4 (English) (1982) p. 61.
12. K. H. HELLWEGE, R. KAISER and K. KUPHAL, *Kolloid-z* **157** (1958) 27.
13. C. L. LOECHELT, E. M. WOO and J. C. SEFERIS, *SPE ANTEC Technical Papers,* **34** (1988) p. 1645.
14. C. B. BUCKNALL and I. K. PARTRIDGE, *Polymer* **24** (1983) 639.

Received 1 May
and accepted 12 September 1991